Available online at www.sciencedirect.com
SCIENCE DIRECT®
Polymer 45 (2004) 2249–2260
polymer
www.elsevier.com/locate/polymer

Morphology and properties of thermoplastic polyurethane nanocomposites incorporating hydrophilic layered silicates

Bradley Finnigan, Darren Martin*, Peter Halley, Rowan Truss, Kayleen Campbell

Divisions of Chemical and Materials Engineering, The University of Queensland, St Lucia, QLD, Brisbane 4072, Australia

Received 22 October 2003; received in revised form 19 January 2004; accepted 28 January 2004

Abstract

Hydrophilic layered silicate/polyurethane nanocomposites were prepared via twin screw extrusion and solvent casting. Good dispersion and delamination was achieved regardless of processing route, illustrating that the need for optimised processing conditions diminishes when there is a strong driving force for intercalation between the polymer and organosilicate. Evidence for altered polyurethane microphase morphology in the nanocomposites was provided by DMTA and DSC. WAXD results suggested that the appearance of an additional high temperature melting endotherm in some melt-compounded nanocomposites was not due to the formation of a second crystal polymorph, but rather due to more well-ordered hard microdomains. Solvent casting was found to be the preferred processing route due to the avoidance of polyurethane and surfactant degradation associated with melt processing. While tensile strength and elongation were not improved on organosilicate addition, large increases in stiffness were observed. At a 7 wt% organosilicate loading, a 3.2-fold increase in Young's modulus was achieved by solvent casting. The nanocomposites also displayed higher hysteresis and permanent set.

Keywords: Nanocomposites; Polyurethane; Processing

1. Introduction

Thermoplastic polyurethanes (TPUs) are linear block copolymers consisting of alternating hard and soft segments. The hard segment is composed of alternating diisocyanate and chain extender molecules (i.e. diol or diamine), while the soft segment is formed from a linear, long-chain diol. Phase separation occurs in TPUs because of the thermodynamic incompatibility of the hard and soft segments. The segments aggregate into microdomains resulting in a structure consisting of glassy, hard domains, and rubbery, soft domains, that are below and above their glass transition temperatures at room temperature, respectively. The hard domains gain their rigidity through physical crosslinking (hydrogen bonding between hard segments), and provide filler-like reinforcement to the soft segment. The complex microstructure of TPUs and its relationship to the macroscopic properties has fascinated researchers for decades [1–10], and continues to do so [11,12].

The incorporation of nano-sized layered silicates into polymer hosts has led to reports of improved mechanical, thermal, and barrier properties, among others [13–17]. Although the mechanisms behind these improvements are not well understood at present, it is evident that the altered properties of these materials are related to changes in polymer molecular dynamics [18,19] and crystallinity [20], in addition to traditional filler reinforcement. The exfoliated structure is often the most desirable because the resulting nanocomposite properties are isotropic and the high aspect ratio and surface area of the dispersed particles is fully utilised. Numerical self-consistent field calculations suggest that end-functionalised polymers or block copolymers are well suited to achieve exfoliation [21]. For this to happen, the polymer must have a fragment that is highly attracted to the silicate surface and another fragment that is not attracted in order to push the platelets apart to regain entropy. Exfoliation could therefore be theoretically achieved by preferentially attracting either the soft or hard segment of a TPU to the silicate surface. In reality, it is more likely that exfoliation of layered silicates in TPUs will be achieved by using surfactants with polar functionality to attract the hard segments [22]. Computational work by Balazs et al. [23] on phase-separating block copolymers has indicated that the

* Corresponding author. Tel.: +61-7-33654176; fax: +61-7-33654199.
E-mail addresses: dmartin@minmet.uq.edu.au (D. Martin).

0032-3861/$ - see front matter © 2004 Elsevier Ltd. All rights reserved.
doi:10.1016/j.polymer.2004.01.049

introduction of nanofillers that preferentially interact with one of the polymer phases can induce large changes in morphology. TPUs represent an ideal system to study the above-mentioned concepts.

The study of polyurethane (PU) layered silicate nanocomposites is still relatively immature. PU nanocomposites have previously been prepared by techniques including solvent casting [24,25] and in situ polymerisation [26,27] and improvements in barrier [25,28–30] and mechanical properties [28,31] have been reported. To date, there have been no reports in the literature of TPU nanocomposites being prepared by twin-screw extrusion, and there has been no thorough investigation into the effect of layered silicates on the microphase morphology. In this paper we present our initial experiments aimed at furthering the understanding of PU nanocomposites. TPU nanocomposites were prepared by both twin-screw extrusion and solvent casting using a commercially available silicate with polar functionality to promote exfoliation. The effect of well-dispersed layered silicates on the morphology and properties of TPUs with discrete and co-continuous microdomain morphologies was investigated.

2. Experimental

2.1. Materials and preparation

Two TPUs were employed in this study. A soft elastomer of Shore Hardness 80A (SPU) and a hard elastomer of Shore Hardness 55D (HPU). Both formulations consisted of a 1000 g/mol poly(tetramethylene oxide) (PTMO) soft segment with a 4,4′-methylene diphenyl diisocyanate (MDI) and 1,4-butanediol (BDO) hard segment. The hard segment concentrations of the SPU and HPU were 35 and 55 wt%, respectively. The TPUs were supplied by Urethane Compounds, Melbourne.

The organically-modified layered silicate used in this study was Cloisite 30B (30B) (Southern Clay Products). The Cloisite series of organosilicates are based on a natural montmorillonite with a cation exchange capacity of 0.92 meq/g. 30B has a 0.9 meq/g methyl bis-2-hydroxyethyltallow ammonium modification, and the tallow composition is ca. 65% C_{18}, 30% C_{16}, and 5% C_{14}. 30B was dried in a vacuum oven at 80 °C for 12 h prior to use.

Melt compounding (MC). PU and 30B were compounded in a ThermoHaake minilab twin screw extruder. A screw speed of 40 rpm was employed and a barrel temperature of 210 and 220 °C was used for the SPU and HPU, respectively. The extrudate was compression moulded at the same temperatures for 3 min.

Solvent casting (SC). A 5 wt% solution of dried organosilicate in toluene was ultrasonicated at 20 kHz for 2 min before being added to a 5 wt% solution of PU in dimethyl acetamide (DMAc). The combined solution was then mixed vigorously for 1 min in a high-shear homogeniser, followed by stirring for 1 h at room temperature with a magnetic stirrer. The mixture was then ultrasonicated for 2 min and films were immediately cast onto glass plates. The films were dried at 50 °C for 36 h under a nitrogen purge and subsequently for 12 h under vacuum.

The solvent cast and melt compounded films were then annealed under vacuum at 80 °C for 12 h and left for 1 month prior to characterisation. Nanocomposites with organosilicate loadings of 3 and 7 wt% were prepared.

2.2. Characterisation

Differential scanning calorimetry (DSC) measurements were performed on a TA Instruments 2920 MDSC. The sample weight was approximately 10 mg and the heating rate employed was 10 °C/min.

Dynamic mechanical measurements were made using a Rheometric Scientific dynamic thermal mechanical analyser (DMTA IV) equipped with tensile head and reducing force option. Analysis was performed using a frequency of 2 Hz and a heating rate of 2 °C/min.

Wide-angle X-ray diffraction (WAXD) analysis was carried out on a Bruker D8 Advance X-ray diffractometer using Cu K_α radiation generated at 40 kV and 30 mA. Samples were scanned at 2.4°/min in the range of $2\theta = 1° - 40°$ using a step size of 0.02°. The 30B powder was lightly pressed and flattened to obtain a smooth surface prior to testing.

Transmission electron microscope (TEM) samples were cut on a Leica Ultracut S ultramicrotome with a glass knife at − 100 °C and collected on 400 mesh copper grids. Images were obtained using a JEOL JEM 1010 TEM operated at 100 keV.

Thermogravimetric analysis (TGA) of 30B was carried out on a Shimadzu TGA 50 under an air atmosphere. A heating rate of 10 °C/min and sample weight of approximately 10 mg were used.

Molecular weights of the PUs were determined by gel permeation chromatography (GPC) on a Waters Alliance 2690 Separations Module. HPLC grade DMAc containing 0.03 wt% LiCl was used as eluent and two Styragel columns (3 HT and 6E HT: 500–30,000 and 5000-1 × 10^7 effective MW range, respectively) were used for separation. Polystyrene standards were used for calibration (Pressure Chemical Company).

Tensile and hysteresis tests were carried out on an Instron model 4505 universal testing machine using 5 replicates of each material. Dumbbells approximately 1 mm thick were punched from an ATSM D-638-M-3 die. A crosshead speed of 5 mm/min was employed and pneumatic grips were used to prevent slippage. The hysteresis values reported were measured on the 5th loading–unloading cycle. Permanent set was taken as the strain at which a zero load is measured on the unloading cycle.

3. Results and discussion

3.1. PU molecular weight

The number average molecular weights (M_n) and polydispersity indices (PDI) of the as-received, solvent cast, and melt compounded PUs are given in Table 1. The molecular weights of the nanocomposites were not determined to eliminate the possibly of layered silicates entering the separation columns. A significant decrease in M_n occurred during both the solvent casting and melt compounding procedures. The ultrasonic probe has been identified as the cause for the reduction in molecular weight in the solvent cast materials. Care must be taken when melt processing TPUs because they are susceptible to thermal and thermo-oxidative degradation in the temperature range required to process them [32,33]. Small extruders have been reported to impose a harsher environment on polymers than their larger counterparts because the surface area to volume ratio increases with decreasing extruder size [34]. In addition to the small extruder used in this study, the PUs did not contain additives to reduce degradation.

3.2. Nanocomposite structure

WAXD patterns of the nanocomposites based on the SPU and HPU are shown in parts (a) and (b) of Fig. 1, respectively. In these systems it is likely that the hard segments are preferentially attracted to the silicate surface, and that the soft segments push the platelets apart to regain entropy [21]. The appearance of a diffraction peak/shoulder at $2\theta = \sim 2.5°$ corresponds to a basal spacing increase from 1.85 to 3.85 nm and 3.95 nm for the HPU and SPU nanocomposites, respectively. These results suggest that there is a slightly larger basal spacing increase when 30B is dispersed in the SPU. The SPU contains a higher fraction of the entropic soft segment, which may account for the larger spacing. The low peak intensities and range of basal spacings suggests that these nanocomposites contain portions of both intercalated and exfoliated clay platelets. The larger ratio of d_{001}/d_{002} and the appearance of diffuse shoulders (as opposed to diffuse peaks) in the melt compounded materials, indicates that the clay platelets are less ordered when the nanocomposites are prepared via extrusion. It should be noted that thicker specimens were tested for the melt-compounded materials resulting in the observed higher intensities.

Table 1
Molecular weight of host polymers

	SPU		HPU	
	M_n	PDI	M_n	PDI
AR[a]	216,000	1.8	85,000	2.0
SC[b]	121,000	1.7	82,000	2.1
MC[c]	66,000	2.0	59,000	1.9

[a] As-received PU.
[b] Solvent cast.
[c] Melt compounded.

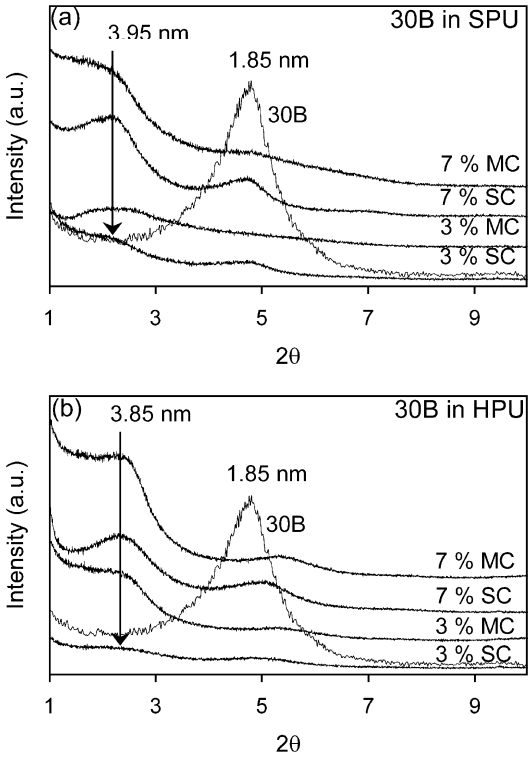

Fig. 1. WAXD intensity profiles of (a) SPU, and (b) HPU nanocomposites.

TEM images of the SPU and HPU nanocomposites are displayed in Figs. 2 and 3, respectively. These images reveal that the clay platelets are well dispersed, and small clusters of intercalated silicates and a portion of exfoliated silicates are visible in all images. The effectiveness of both processing methods illustrates that if there is a good interaction between the polymer and filler, the need for an optimised processing procedure is diminished. The good degree of exfoliation achieved in this system can be attributed to the strong driving force for intercalation provided by the potential for hydrogen bonding between the polymer and filler. The hydroxyl groups on 30B are capable of forming hydrogen bonds with the hard segments, and to a lesser extent the soft segment ether oxygens. On the basis of these images and the WAXD patterns, it would appear that while both processing routes were effective, slightly better dispersion and delamination was achieved via melt compounding. This result can be attributed to the higher shear stresses involved with twin-screw extrusion, and to the absence of the slow solvent evaporation step, during which clay platelet reorganisation can take place long after the cessation of shear.

As mentioned in the Section 2 the 30B-toluene solution was exposed to ultrasound prior to being added to the PU solutions. The sonication of this solution led to the formation of a stable gel as a result of the clay exfoliating. In agreement with Zhong and Wang's results [35], we have

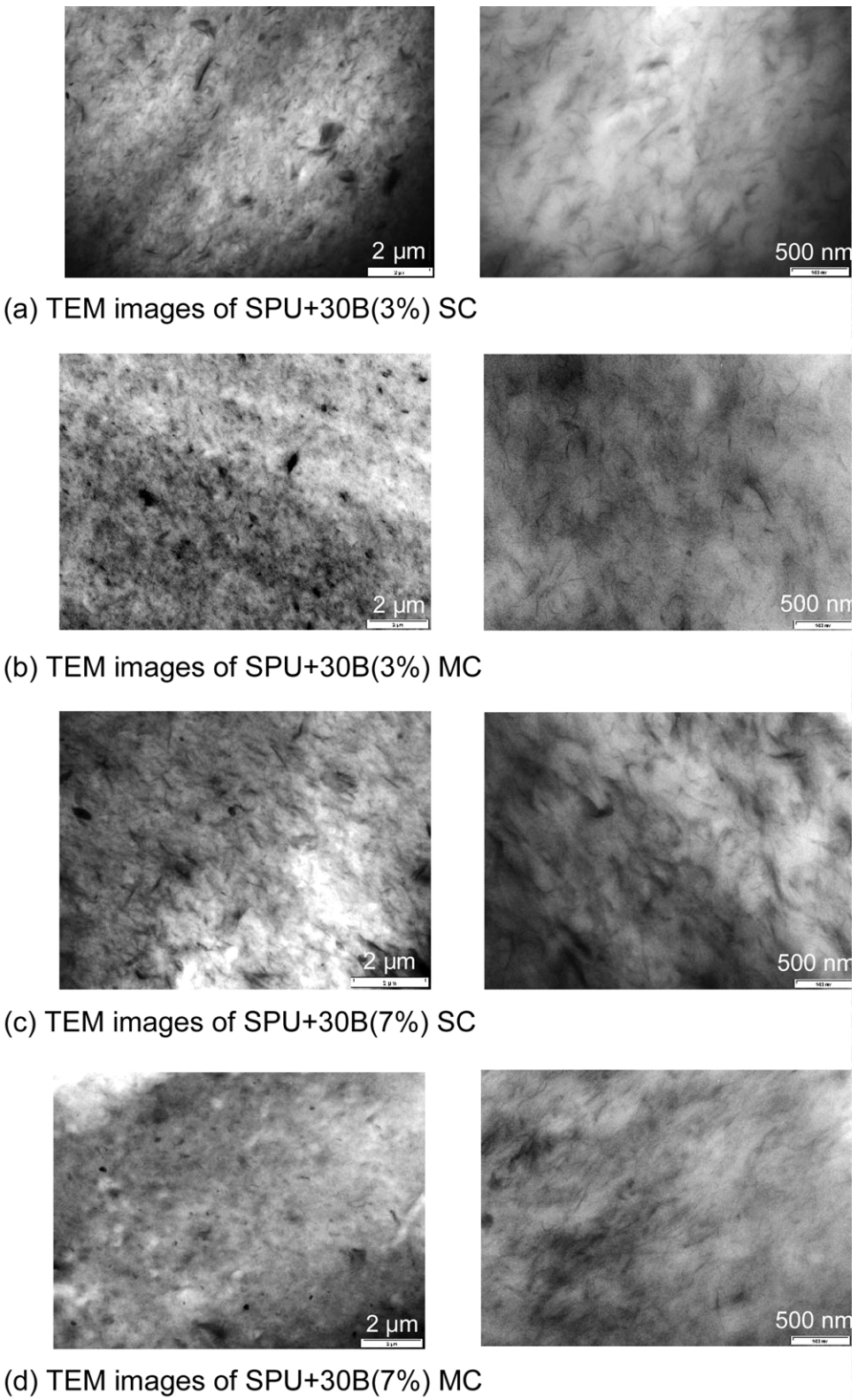

Fig. 2. TEM images of 30B in SPU (a) 3% SC. (b) 3% MC. (c) 7% SC. (d) 7% MC.

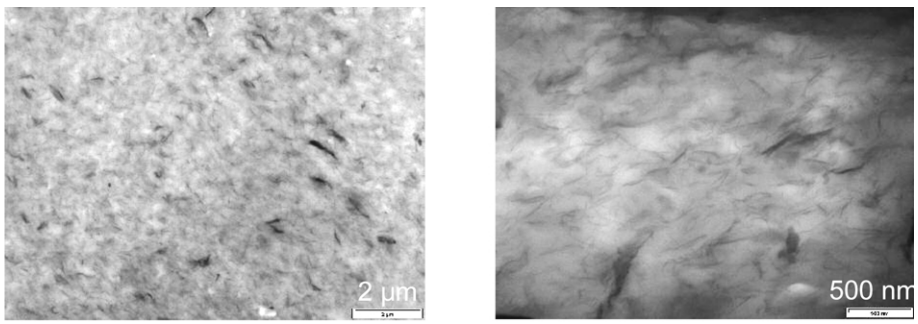

(a) TEM images of HPU+30B(3%) SC

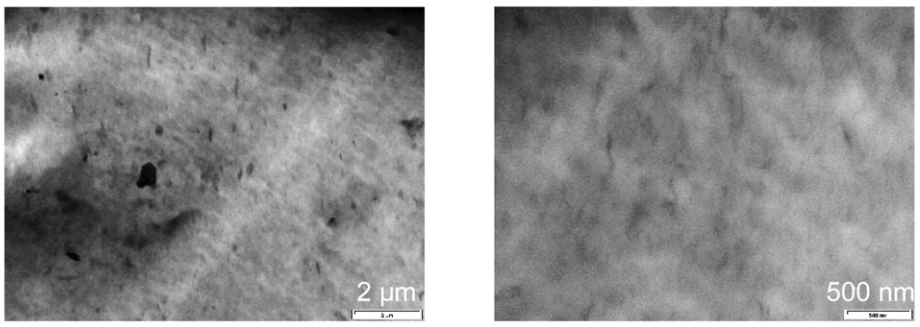

(b) TEM images of HPU+30B(3%) MC

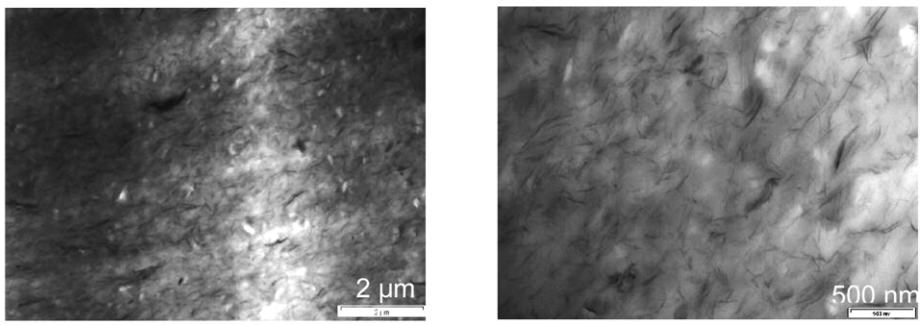

(c) TEM images of HPU+30B(7%) SC

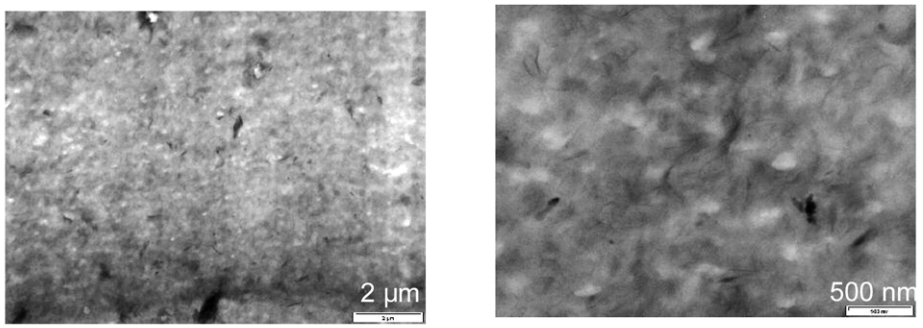

(d) TEM images of HPU+30B(7%) MC

Fig. 3. TEM images of 30B in HPU (a) 3% SC. (b) 3% MC. (c) 7% SC. (d) 7% MC.

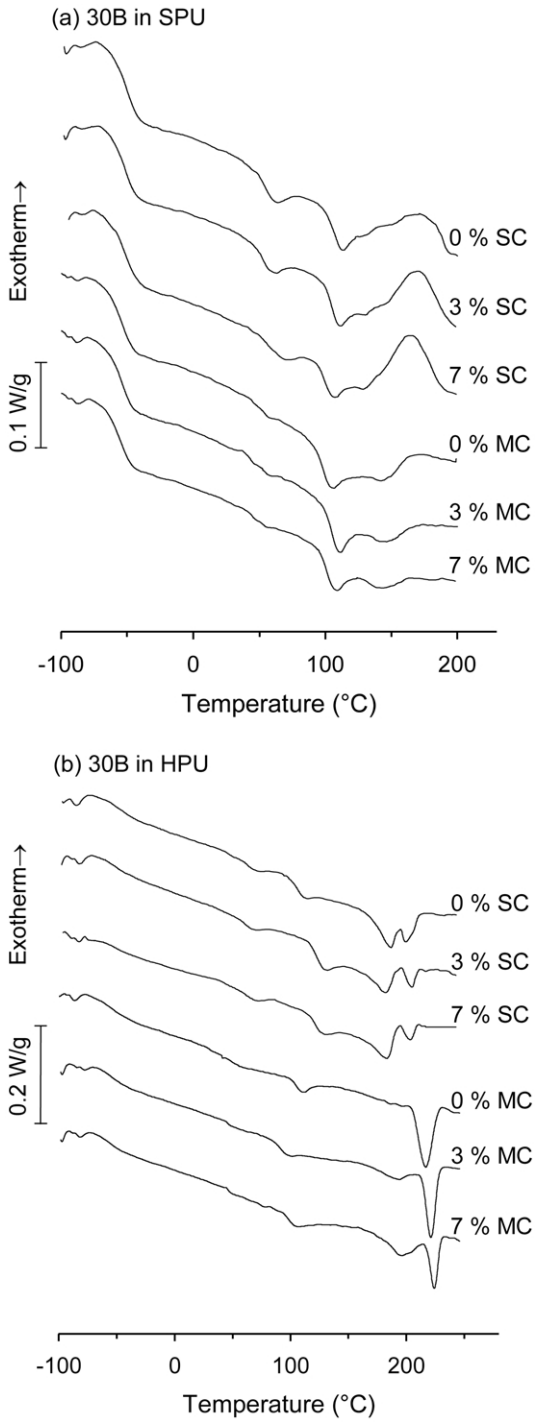

Fig. 4. DSC thermograms of (a) SPU, and (b) HPU materials.

found the choice of dispersing solvent critical to inducing clay exfoliation with ultrasound.

3.3. Differential scanning calorimetry

DSC thermograms of the SPU materials are shown in Fig. 4(a), and a summary of the DSC features is given in Table 2. A strong soft segment glass transition at approximately −55 °C is evident in all materials. DMTA provides a more sensitive measure of this transition, and these results are discussed below. Annealing studies by Martin et al. [9,36] on a series of model compounds provided strong evidence to suggest that the multiple endothermic behaviour of TPUs is a result of the disruption of specific hard segment length populations. Martin et al. identified five endotherms resulting from the disordering of predominantly single MDI, MDI_2BDO, MDI_3BDO_2, MDI_4BDO_3, and MDI_5BDO_4 hard segments. These endotherms were labelled $T1$(50–70 °C), $T2$(100–180 °C), $T3$(190–210 °C), $T4$(211–217 °C), and $T5$(222–230 °C). The endotherms identified in this study have been labelled in keeping with this nomenclature, however the assignment of endotherms to specific hard segment length populations is limited here because of the non-ideal nature of the TPUs employed.

A $T1$ endotherm is observable at approximately 60 °C in the SPU materials prepared by solvent casting. This endotherm can be attributed predominantly to the disordering of hard segments consisting of single MDI units. Eisenbach et al. [37] suggested that in polyetherurethanes this endotherm could be attributed to the disordering of non-ideally packed N–H…C=O hard segments in the interfacial region between the soft and hard phases. The absence of this endotherm in the melt-compounded materials provides evidence for improved phase separation, and hence a narrower and more ordered interfacial region. The SPU materials also exhibit a bimodal $T2$ endotherm that can be attributed to the disruption of various degrees of short-range hard segment order, due to the distribution in hard segment lengths [36,38]. The first of the $T2$ endotherms is related to the annealing temperature and occurs at 100–110 °C, approximately 20–30 °C above the annealing temperature [6,36,38]. Annealing at higher temperatures results in the merging of these two peaks (thermograms not shown). A broad exotherm is observable immediately after the $T2$ endotherms in the SPU materials prepared by solvent casting. It is believed that this exotherm is not a result of a crystallisation process because there are no subsequent melting endotherms in the DSC traces. Instead, this exotherm may be related to a reduction in free energy brought about by the hard segments gaining sufficient mobility to phase separate and reduce interfacial area. Ongoing studies hope to elucidate the exact nature of this exotherm.

DSC thermograms of the materials based on the HPU are presented in Fig. 4(b). Soft microdomain glass transitions are very broad and weak in the HPU series because the co-continuous microstructure and higher hard segment crystallinity of this PU imposes restrictions on molecular motion.

As with the SPU series, a $T2$ endotherm is observed at approximately 20–30 °C above the annealing temperature, and a $T1$ endotherm is also evident for the materials prepared by solvent casting. The smaller size of these endotherms, compared to that displayed by the SPU materials, is a result of the HPU containing fewer short

Table 2
Summary of DSC heating curves

	30B (wt%)/method	$T_{g(soft)}$ (°C)	Endotherm peaks				Hard phase ΔH (J/g)[a,b]	Exotherm	
			$T1$ (°C)	$T2$ (°C)	$T3$ (°C)	$T4$ (°C)		Peak (°C)	ΔH (J/g)[b]
SPU	0% SC	−52	68	113 130	–	–	21.3 ± 3.6	177.5	5.3 ± 0.9
	3% SC	−52	70	114 130	–	–	19.9 ± 1.6	165	5.3 ± 2.8
	7% SC	−52	68	112 136	–	–	22.8 ± 3.7	165	4.1 ± 2.1
	0% MC	−55	–	107 144	–	–	27.5 ± 5.5	–	–
	3% MC	−55	–	113 147	–	–	30.3 ± 1	–	–
	7% MC	−55	–	110 147	–	–	35.1 ± 6.9	–	–
HPU	0% SC	–	67	111	187 202	–	23.6 ± 5	–	–
	3% SC	–	64	120	183 205	–	19.5 ± 2.3	–	–
	7% SC	–	67	123	185 205	–	22.8 ± 4	–	–
	0% MC	–	–	109	–	216	22.5 ± 4.7	–	–
	3% MC	–	–	100	194	221	24.5 ± 5.8	–	–
	7% MC	–	–	105	198	224	26.1 ± 5	–	–

[a] Enthalpy of fusion values are the sum of the $T1$–$T4$ melting enthalpies.
[b] Enthalpies were calculated per gram of hard segment (not per gram of sample).

hard segments [9]. The HPU exhibits a $T4$ melting endotherm centred at 216 °C when prepared via melt compounding. This endotherm can be attributed to the disruption of predominantly MDI_4BDO_3 and MDI_5BDO_4 hard segment structures. When the HPU is prepared by solvent casting a $T4$ endotherm is not observed. The melting temperature of the longer hard segments is depressed, and instead a bimodal $T3$ endotherm is observed. The small fraction of hard segments melting above 200 °C suggests that the hard segments were unable to form crystal structures with long-range order when prepared via solvent casting [38]. A reduction in hard domain order also provides further evidence that the solvent cast materials are not as well phase separated as the melt compounded materials.

Within the range of experimental error, the addition of 30B did not affect the enthalpy associated with the thermal transitions discussed thus far. There was however a significant change in the hard domain order of the HPU nanocomposites prepared by melt compounding. When 30B is melt compounded with the HPU, the $T4$ peak splits into two endotherms. The large polymer-filler interface induces the formation of both lower and higher melting temperature structures that are assigned as $T3$ and $T4$ peaks, respectively in Table 2. Chain packing and folding of a portion of the hard segments is apparently hindered in the melt compounded HPU by the addition of the layered silicates, resulting in the low temperature $T3$ melting structure. The more ordered $T4$ crystal structure with improved thermal stability may be forming at the polymer-filler interface. As the silicate content increases from 3 to 7 wt% the size of the more thermally stable $T4$ peak decreases, this may be due to the silicates imposing spatial restrictions and/or reducing the mobility of the crystallisable hard segments capable of forming this structure. Either of these phenomena would coincide with the observed increase in the size of the low temperature $T3$ melting peak with increasing filler content.

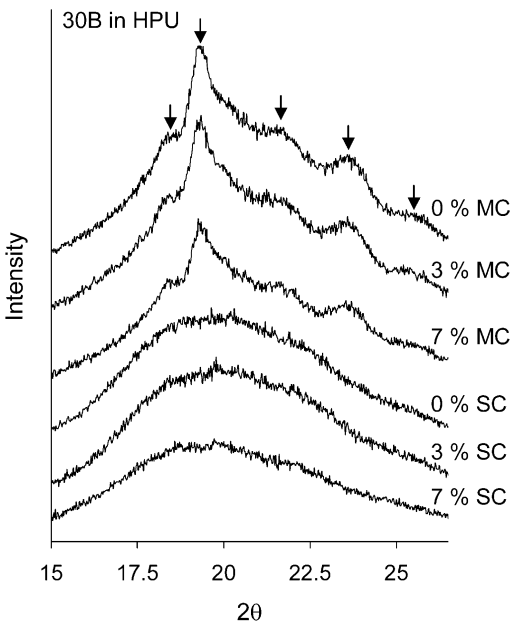

Fig. 5. WAXD patterns of materials based on the HPU.

Table 3
Reported lattice spacings (Å) for MDI/BDO crystals

HPU series (MC)[a]			4.81	4.6			4.12		3.77	3.48	
Koberstein and Galambos type I [39]	7.70	4.93	4.77			4.25		3.92		3.59	3.33
Koberstein and Galambos type II [39]		5.00		4.61	4.43		4.13		3.74	3.47	
Briber and Thomas type I [41]	7.70	5.01						3.89		3.53	3.33
Briber and Thomas type II [40]		4.90		4.62	4.45		4.12		3.77	3.49	
Briber and Thomas type III [40]	7.7	5.1					4.12	3.86	3.79	3.56	3.34
		4.99					4.07				

[a] SPU and solvent cast materials did not display distinct WAXD peaks.

Bearing these results in mind, WAXD was employed to determine whether the splitting of the *T*4 endotherm into two peaks was a consequence of the layered silicates aiding the formation of a second MDI/BDO polymorph, or simply inducing different degrees of ordering of the same crystal type. The WAXD patterns are shown in Fig. 5 and the lattice spacings are reported in Table 3. The lattice spacings present in the melt compounded HPU series are consistent with Type II MDI/BDO crystals [39,40]. The layered silicates therefore do not seem to favour the formation of a second polymorph, which can be seen in nylon 6 for example [20].

The weak intensity of the hard segment crystal peaks reflects the low degree of crystallinity and high level of imperfection present in the melt compounded materials. This level of imperfection is not unexpected given the nature of the polyurethanes used in this study. To assist the formation of well-ordered MDI/BDO crystals it is beneficial to prepare polyurethanes with a narrow hard segment molecular weight distribution [4] and to use severe annealing conditions [40,42]. The absence of hard segment crystal peaks for the solvent cast series is in accordance with the DSC results that predicted the absence of long-range order.

3.4. Dynamic mechanical properties

The dissipation factor (tan δ) of the materials based on the SPU and HPU are presented as a function of temperature in parts (a) and (b) of Fig. 6, respectively. The tan δ peak is associated with the soft segment glass transition temperature (T_g), and the peak positions are given in Table 4. The soft segment T_g of the host polymers occurs at a higher temperature when prepared by solvent casting. This indicates that there are more hard segments present in the soft phase hindering molecular motion. The solubility parameter of DMAc is between that of PTMO and MDI/BDO as shown in Table 5 [43,44]. As a result the hard and soft segments may be more compatible in solution leading to a reduction in phase separation in the PUs prepared by solvent casting. This idea is not unreasonable considering that compatibilising solvents are used to assist in the polymerisation of PUs whose monomers have large differences in solubility parameters [43]. Addition of 30B resulted in an increase in T_g and a reduction in damping capacity in both the solvent cast and melt compounded materials. This is a consequence of the well-dispersed and

Table 4
Glass transition temperatures determined from DMTA

	30B Content (wt%)	$T_{g(soft)}$ (°C)		$T_{g(hard)}$ (°C)	
		MC[a]	SC[b]	MC[a]	SC[b]
SPU	0	−39	−37	–	–
	3	−38	−34	–	–
	7	−38	−33	–	–
HPU	0	−34	−24	66	66
	3	−33	2	66	66
	7	−31	3	72	66

[a] Melt compounded.
[b] Solvent cast.

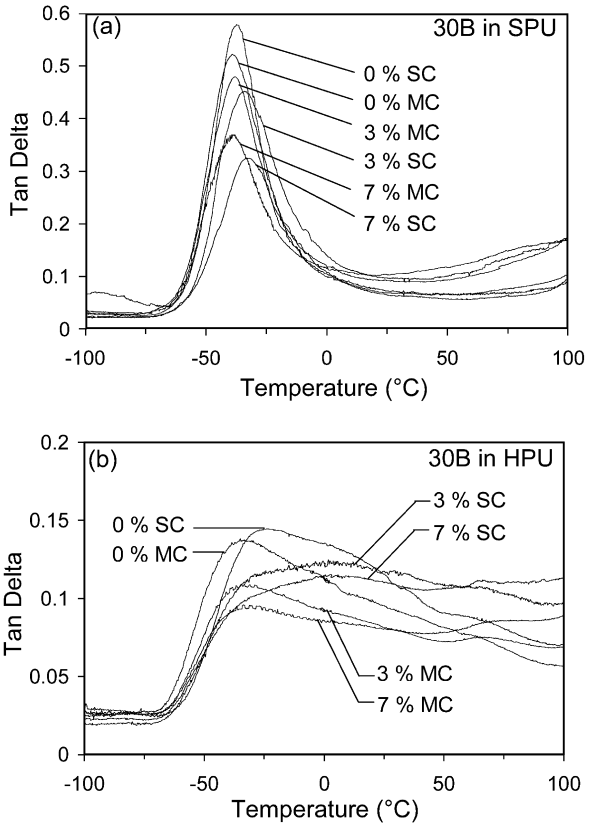

Fig. 6. Dissipation factor (tan δ) of (a) SPU, and (b) HPU materials as a function of temperature.

Table 5
Solubility parameters

Compound	Solubility parameter, δ, $(cal/mL)^{1/2}$
BDO	13.98 ± 0.05[a]
$(MDI\text{-}BDO)_1$ hard segment	12.2–12.7[a]
DMAc	10.8[b]
MDI	9.94 ± 0.08[a]
PTMO (MW 1000)	9.55 ± 0.09[a]

[a] From Gunatillake et al. [43].
[b] From polymer handbook [44].

delaminated silicates restricting molecular motion. The relatively strong polymer-filler interaction present in this system, resulting from the potential for hydrogen bonding between the polymer and silicate, is also expected to contribute to the restricted molecular motion [18].

In both the SPU and HPU the increase in soft segment T_g with increasing 30B content is more significant in the materials prepared by solvent casting. The WAXD and TEM results presented earlier suggest that this is not a result of the silicates being dispersed and delaminated more effectively in the solvent cast materials. Therefore it can be postulated that 30B reduces the extent of microphase separation in DMAc solution. Small-angle X-ray and neutron scattering studies are planned to further elucidate this phenomenon.

The high temperature side of the tan δ peak is associated with the relaxation of the interfacial region between the hard and soft phases. The unusually low gradient of the high temperature side of this peak observed for the HPU materials suggests that there is a thick interfacial region. It is likely that the one step bulk synthesis of the HPU, and the processing-induced degradation, resulted in a polymer with a broad hard segment molecular weight distribution that hindered hard domain packing [4,33,45]. The solvent cast materials display an even broader peak that is believed to be a result of reduced microphase separation.

A hard segment glass transition can be seen in the HPU materials at approximately 60–70 °C. However the weak signal in this region prevents a comprehensive analysis of this transition being made.

The storage modulus (E') curves of the SPU and HPU materials are presented in parts (a) and (b) of Fig. 7, respectively. The storage modulus of the HPU materials is an order of magnitude higher than that of the SPU materials at room temperature. This difference is a consequence of the higher hard segment content and co-continuous microphase texture reinforcing the soft phase. The well-dispersed and delaminated 30B platelets restrict molecular motion resulting in an increase in storage modulus regardless of host polymer or processing route.

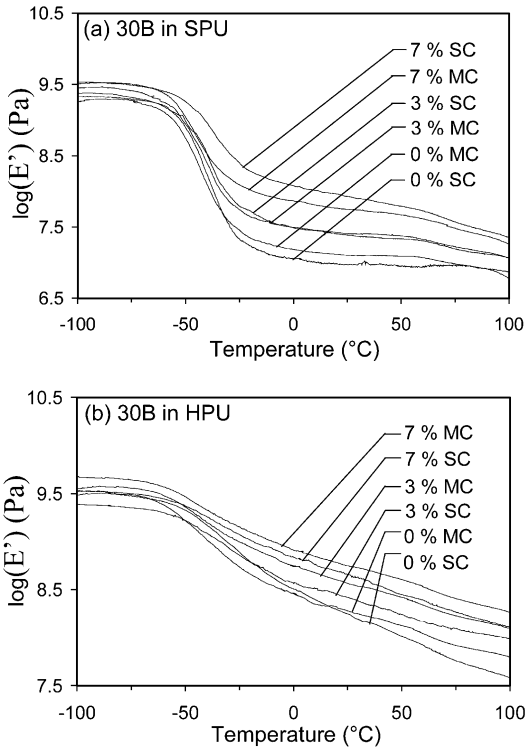

Fig. 7. Storage modulus (E') of (a) SPU, and (b) HPU materials as a function of temperature.

3.5. Mechanical properties

A summary of the tensile properties of the host polymers and nanocomposites are provided in Table 6. As observed with the storage modulus results, the Young's modulus of the HPU materials is significantly higher than the SPU

Table 6
Summary of tensile properties

	30B Content (wt%)	Solvent cast			Melt compounded		
		Young's modulus (MPa)	Tensile strength (MPa)	Fail strain (%)	Young's modulus (MPa)	Tensile strength (MPa)	Fail strain (%)
SPU	0	7.5 ± 0.2	45 ± 4	1136 ± 48	7.2 ± 0.6	21 ± 4	1445 ± 97
	3	13.8 ± 1	31 ± 4	1109 ± 12	11.4 ± 1	22 ± 3	1163 ± 125
	7	24 ± 0.2	21 ± 4	1030 ± 92	19.3 ± 1	7 ± 1	568 ± 71
HPU	0	50 ± 5	58 ± 5	898 ± 64	61 ± 5	44 ± 2	776 ± 45
	3	86 ± 2	44 ± 1	808 ± 34	81 ± 3	20 ± 5	283 ± 158
	7	134 ± 10	34 ± 2	704 ± 24	119 ± 13	15 ± 2	100 ± 90

materials. Once again this is result of the higher hard segment content and co-continuous microphase structure. The modulus of the host HPU polymer is higher when prepared by melt compounding compared to solvent casting, probably because of the higher hard segment crystallinity [4]. The modulus of the host SPU polymer was similar for the two processing methods despite having different degrees of microphase separation. Incorporation of 30B into the host polymers led to large increases in stiffness with increasing inorganic content, in agreement with the storage modulus results obtained from DMTA. The largest increase in modulus (3.2-fold) was achieved at a 7 wt% loading of 30B in the SPU prepared by solvent casting. The stiffness of the SPU was enhanced more than the HPU on silicate addition because the SPU contains a higher fraction of rubbery PTMO. Increases in modulus result from the mismatch in the elastic constants of the polymer and filler [46], and for this reason polymers in the rubbery state are impacted more by nanofiller reinforcement than glassy polymers [47]. Understanding the differences in E' and Young's modulus between the solvent cast and melt compounded nanocomposites is difficult, because in addition to the degree of silicate delamination and polymer molecular weight, the size, shape, and order of the hard microdomains is important [1,2]. Future efforts will focus on identifying the microdomain textures of these materials.

Tensile curves of the SPU and HPU series of materials are presented in Fig. 8. The curves of the solvent cast specimens have been offset for clarity. Considering the host polymers initially, it is clear that the ultimate tensile strength achieved by solvent casting is significantly higher. The reduced strength of the melt compounded polymers can be mostly attributed to degradation that occurred during extrusion and compression moulding. The solvent cast materials exhibit a larger upturn in the tensile curve that is attributed to chain stretching and soft segment crystallisation in thermoplastic polyurethane elastomers. In addition to degradation, the cause of the reduced upturn in the melt compounded materials may be a result to their higher hard segment crystallinity, which is believed to impose restrictions on soft segment crystallisation [4]. The HPU displays a higher yield plateau when melt compounded, providing further evidence for higher phase separation and hard segment crystallinity being achieved with this processing method.

The good dispersion and delamination of 30B in both PUs led to a reduction in ultimate tensile properties with increasing filler content. The reduction in ultimate tensile properties of the melt compounded nanocomposites can be primarily attributed to a reduction in PU molecular weight brought about by degradation of the 30B surfactant. The temperature required to melt process the PUs used in this study was higher than the onset of the 30B surfactant degradation temperature (~200 °C). Recently, the 30B surfactant degradation products have been identified in our laboratories, and this work will be reported elsewhere. Some

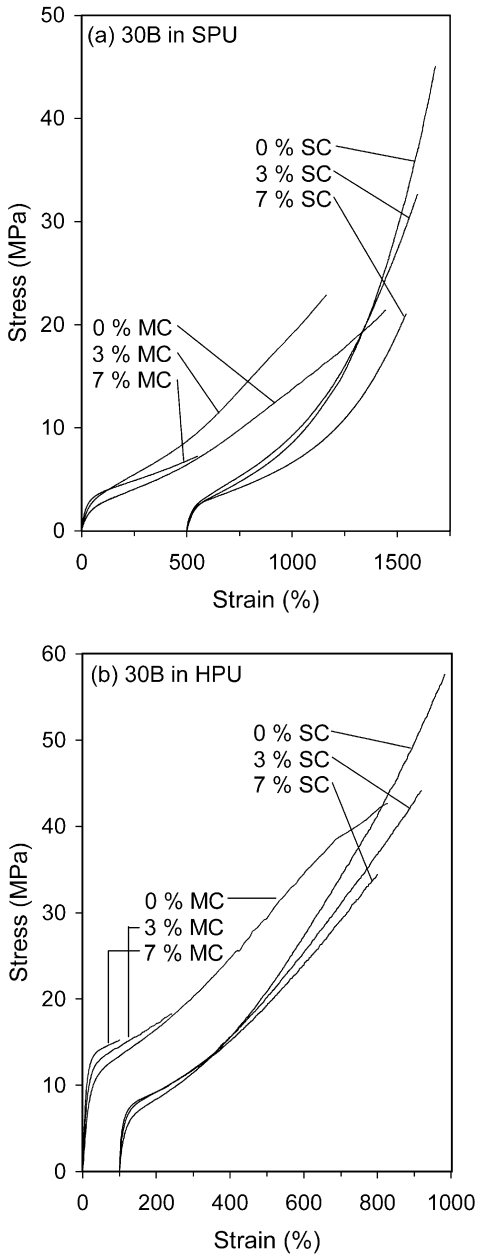

Fig. 8. Tensile curves of (a) SPU, and (b) HPU materials.

of the degradation products, such as alkenes [48], are known to react readily with isocyanates that are present in melt processing due to the normal urethane dissociation and recombination reactions that occur above 170 °C [33,36]. Such reactions are believed to have decreased the molecular weight leading to reduced strength and elongation, particularly in the HPU materials because it was necessary to process them at 220 °C. The one exception was the SPU nanocomposite containing 3 wt% 30B, which maintained its tensile strength.

The reason for reduced tensile properties in the solvent cast nanocomposites is not clear at this point in time. Possible reasons for reduced tensile properties include altered microphase morphology, excessive polymer-filler

Table 7
Summary of materials under cyclic conditions

	30B (wt%)	Solvent cast				Melt compounded			
		H_{100}[a] (%)	PS_{100}[b] (%)	H_{200}[a] (%)	PS_{200}[b] (%)	H_{100}[a] (%)	PS_{100}[b] (%)	H_{200}[a] (%)	PS_{200}[b] (%)
SPU	0	9 ± 1	13 ± 1	14 ± 1	32 ± 2	11 ± 1	13 ± 1	14 ± 1	35 ± 6
	3	21 ± 1	23 ± 1	24 ± 1	56 ± 5	18 ± 1	24 ± 2	23 ± 1	50 ± 7
	7	29 ± 1	37 ± 1	29 ± 1	81 ± 1	28 ± 2	41 ± 6	30 ± 1	94 ± 11
HPU	0	35 ± 1	33 ± 2	38 ± 1	80 ± 3	30 ± 1	36 ± 1	34 ± 1	98 ± 3
	3	43 ± 1	43 ± 1	43 ± 1	103 ± 2	33 ± 1	48 ± 1	35 ± 1	117 ± 2
	7	48 ± 1	58 ± 1	45 ± 1	120 ± 3	38 ± 3	57 ± 3	–[c]	–[c]

[a] Hysteresis (H) calculated on 5th loading–unloading cycle to 100 and 200% strain, respectively.
[b] Permanent set (PS) was taken as the strain at which zero load was measured on the 5th unloading cycle to 100 and 200% strain, respectively.
[c] Samples failed prior to 200% strain.

interaction [48], and an inhibition of the usual morphological changes that accompany deformation in segmented polyurethanes (i.e. hard domain rotation, interchain slippage, fibrillation, and soft segment crystallisation) [1,8]. Future studies hope to elucidate the reason for the reduction in ultimate tensile properties. It is also worth mentioning that the layered silicates used in this study (~200 nm) are very large relative to the microphase texture of the PUs (<20 nm).

Hysteresis was calculated on the 5th cycle to observe the behaviour of the nanocomposites under cyclic conditions. The hysteresis and permanent set results are presented in Table 7. Interconnecting hard domains undergo plastic deformation at lower strains, resulting in the observed higher hysteresis and permanent set values for the HPU materials. The addition of 30B resulted in an increase in hysteresis and permanent set. Energy is required to orientate the silicate platelets and the platelets are unable to return to their original positions. This in turn hinders the ability of the elastomers to relax. The increase in hysteresis and permanent set with filler content was more significant for the SPU, which had relatively low initial values because of its discrete microdomain structure.

4. Conclusions

Cloisite 30B dispersed and delaminated effectively in both of the segmented polyurethanes employed in this study, regardless of processing route. This result illustrates that if there is a good driving force for intercalation between the polymer and organosilicate, the need for an optimised processing route is diminished. Addition of 30B led to an increase in soft segment T_g in both PUs, and evidence for altered microphase morphologies was provided. Nanocomposites based on the HPU displayed a high temperature melting endotherm when prepared by melt compounding. WAXD results suggested that this was not due to the formation of a second crystal polymorph, which is observed when layered silicates are added to other polymers such as nylon 6 [20]. While melt compounding offered slightly better silicate dispersion than solvent casting, solvent casting must be the preferred processing route for these materials due to the elimination of polyurethane and surfactant degradation. Large improvements in stiffness were observed on silicate addition, particularly for the SPU, which contained a higher fraction of soft segment. At a 7 wt% loading of 30B, a 3.2-fold increase in Young's modulus was achieved via solvent casting. The improvement in stiffness can be attributed to the good dispersion and delamination achieved, in addition to the strong interaction between these PUs and 30B. The addition of 30B resulted in a decrease in tensile strength and elongation. At this stage it is unclear why 30B had a detrimental effect on the ultimate tensile properties and future work will aim to address this issue. The addition of layered silicates with high aspect ratios was observed to increase the hysteresis and permanent set of these PU elastomers.

Acknowledgements

The authors wish to thank Dr Pathiraja Gunatillake of CSIRO for helpful discussions, Mr Graham Ruhle for assistance with mechanical testing, and Mr Michael Murphy for assistance with the DMTA. This work was supported by a University of Queensland Postgraduate Research Scholarship.

References

[1] Speckhard TA, Cooper SL. Rubber Chem Technol 1986;59:405.
[2] Wang CB, Cooper SL. Macromolecules 1983;16:775.
[3] Harrell Jr LL. Macromolecules 1969;2:607.
[4] Miller JA, Lin SB, Hwang KKS, Wu KS, Gibson PE, Cooper SL. Macromolecules 1985;18:32.
[5] Bonart R. J Macromol Sci Phys 1968;B2(1):115.
[6] Koberstein JT, Russell TP. Macromolecules 1986;19:714.
[7] Huh DS, Cooper SL. Polym Engng Sci 1971;11:369.
[8] Lee HS, Yoo SR, Seo SW. J Polym Sci, Part B: Polym Phys 1999;37:3233.
[9] Martin DJ, Meijs GF, Renwick GM, McCarthy SJ, Gunatillake PA. J Appl Polym Sci 1996;62:1377.

[10] Martin DJ, Meijs GF, Gunatillake PA, Yozghatlian SP, Renwick GM. J Appl Polym Sci 1999;71:937.
[11] Yeh F, Hsiao BS, Sauer BB, Michel S, Siesler HW. Macromolecules 2003;36:1940.
[12] Gisselfalt K, Helgee B. Macromol Mater Engng 2003;288:265.
[13] Kojima Y, Usuki A, Kawasumi M, Okada A, Fukushima Y, Kurauchi T, Kamigaito O. J Mater Res 1993;8:1185.
[14] Alexandre M, Dubois P. Mater Sci Engng 2000;28:1.
[15] Giannelis EP. Adv Mater 1996;8:29.
[16] LeBaron PC, Wang Z, Pinnavaia TJ. Appl Clay Sci 1999;15:11.
[17] Schmidt D, Shah D, Giannelis EP. Curr Opin Solid State Mater Sci 2002;6:205.
[18] Lu HB, Nutt S. Macromolecules 2003;36:4010.
[19] Kuppa V, Manias E. J Chem Phys 2003;118:3421.
[20] Liu XH, Wu QJ. Eur Polym J 2002;38:1383.
[21] Balazs AC, Singh C, Zhulina E. Macromolecules 1998;31:8370.
[22] Li XC, Ha CS. J Appl Polym Sci 2003;87:1901.
[23] Balazs AC, Ginzburg VV, Qiu F, Peng GW, Jasnow D. J Phys Chem B 2000;104:3411.
[24] Chen TK, Tien YI, Wei KH. Polymer 2000;41:1345.
[25] Xu RJ, Manias E, Snyder AJ, Runt J. Macromolecules 2001;34:337.
[26] Ma JS, Zhang SF, Qi ZN. J Appl Polym Sci 2001;82:1444.
[27] Wang Z, Pinnavaia TJ. Chem Mater 1998;10:3769.
[28] Chang JH, An YU. J Polym Sci, Part B: Polym Phys 2002;40:670.
[29] Tortora M, Gorrasi G, Vittoria V, Galli G, Ritrovati S, Chiellini E. Polymer 2002;43:6147.
[30] Xu RJ, Manias E, Snyder AJ, Runt J. J Biomed Mater Res 2003;64A: 114.
[31] Tien YI, Wei KH. Macromolecules 2001;34:9045.
[32] Shieh YT, Chen HT, Liu KH, Twu YK. J Polym Sci, Part A: Polym Chem 1999;37:4126.
[33] Yang WP, Macosko CW, Wellinghoff ST. Polymer 1986;27:1235.
[34] Whiteside BR, Martyn MT, Coates PD, Greenway G, Allen P, Hornsby P. Polym Process Soc Annu Meeting 2003;19.
[35] Zhong Y, Wang SQ. J Rheol 2003;47:483.
[36] Martin DJ, Meijs GF, Gunatillake PA, McCarthy SJ, Renwick GM. J Appl Polym Sci 1997;64:803.
[37] Eisenbach CD, Baumgartner M, Gunter C. In: Lal J, Mark JE, editors. Advances in elastomers and rubber elasticity. New York: Plenum; 1986. p. 51.
[38] Seymour RW, Cooper SL. Macromolecules 1973;6:48.
[39] Koberstein JT, Galambos AF. Macromolecules 1992;25:5618.
[40] Briber RM, Thomas EL. J Polym Sci, Part B: Polym Phys 1985;23: 1915.
[41] Briber RM, Thomas EL. J Macromol Sci Phys 1983;B22:509.
[42] Quay JR, Sun Z, Blackwell J, Briber RM, Thomas EL. Polymer 1990; 31:1003.
[43] Gunatillake PA, Meijs GF, McCarthy SJ, Adhikari R. J Appl Polym Sci 2000;76:2026.
[44] Brandrup J, Immergut EH, Grulke EA. Polymer handbook, 4th ed. New York: Wiley; 1999.
[45] Peebles LH. Macromolecules 1974;7:872.
[46] Buxton GA, Balazs AC. J Chem Phys 2002;117:7649.
[47] Gersappe D. Phys Rev Lett 2002;89:058301.
[48] Xie W, Gao ZM, Pan WP, Hunter D, Singh A, Vaia R. Chem Mater 2001;13:2979.